Mechanism Generation with Integrated Pressure Dependence: A New Model for Methane Pyrolysis

David M. Matheu,[†,‡] Anthony M. Dean,[§] Jeffrey M. Grenda,[#] and William H. Green, Jr.*[,†]

Department of Chemical Engineering, Massachusetts Institute of Technology, Cambridge, Massachusetts 02139, Department of Chemical Engineering, Colorado School of Mines, Golden, Colorado 80401, and ExxonMobil Research and Engineering Company, Annandale, New Jersey 08801

Received: March 7, 2003; In Final Form: July 22, 2003

Autocatalytic, lower-temperature (≤1100 K) methane pyrolysis has defied mechanistic explanation for almost three decades. The most recent attempt (by Dean in 1990) invoked the chemically activated addition of an allyl radical to acetylene, leading to a cyclopentadiene/cyclopentadienyl chain-branching system that prompted the observed autocatalysis. However, newer, more accurate thermochemical data for the cyclopentadienyl radical render that explanation untenable. A new model for methane pyrolysis is constructed here, using a novel mechanism generation approach that automatically computes any needed rate constants $k(T,P)$ for chemically or thermally activated pressure-dependent reactions. The computer-generated mechanism accurately predicts the observed autocatalysis and concentration profiles without any adjustable parameters. Radical-forming reverse disproportionation reactions—which involve propyne, allene, and fulvene—account for at least half of the experimentally observed autocatalytic effect. Many of these reverse disproportionations were neglected in previous studies. The cyclopentadienyl radical is also important, but it is formed primarily by the chemically activated reaction of propargyl with acetylene. New rate estimates for unimolecular ring-closure reactions of unsaturated radicals are also presented. This approach is the first to incorporate pressure-dependent reactions generally and systematically during computerized mechanism construction. It successfully identifies complex but critical chemical-reaction pathways and autocatalytic loops missed by experienced kineticists.

1. Introduction

1.1. Autocatalytic Behavior in Methane Pyrolysis. Methane pyrolysis has been extensively studied for many decades, both for its potential to convert methane to more valuable hydrocarbons and because of its importance within larger combustion and pyrolysis mechanisms (see, for example, refs 1−13). The pyrolysis of methane often produces large quantities of coke, carbon, and hydrogen, because these are the thermodynamically favored products at almost all practical temperatures.[7] This seriously limits its straightforward industrial application,[10] so that research focuses on novel reactor designs and catalysts that could kinetically trap desirable products before coke and soot dominate (see, for example, Faliks et al.[14]). Thus, proper understanding of the homogeneous gas-phase mechanism of methane pyrolysis is crucial for successful reactor and catalyst design.[2] In addition, the correct modeling of combustion in fuel-rich regimes sometimes requires a methane pyrolysis submechanism.[6]

These demands have driven various attempts at a mechanistic understanding, over a wide range of temperatures and pressures. Beginning in the 1970s, Chen and co-workers performed numerous experiments on methane pyrolysis at lower temperatures and moderate pressures (<1100 K and 0.5−1.0 atm)[15−17] and discovered a sharp autocatalysis at very low methane conversion (<1%) that neither surface reactions nor the then-current gas-phase chemical kinetics models could explain. Indeed, they found autocatalysis to be a general but inexplicable feature of lower-temperature (<1100 K) methane pyrolysis. Roscoe and Thompson attempted to build a small mechanism (using species having three C atoms or less) for the process.[18] Although this mechanism seemed to describe the observed autocatalysis, the reverse rate coefficients were assigned independently from the forward ones. A check of these ratios showed that they were not consistent with the reaction equilibrium constants. When the reverse rate coefficients were made consistent, the predicted autocatalysis virtually disappeared. Thus, lower-temperature methane pyrolysis defied mechanistic explanation, until the work of Dean in 1990.[19]

Dean proposed the importance of cyclopentadiene, formed via the pressure-dependent pathways of reaction 1:

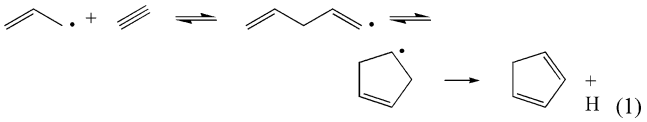

(1)

Cyclopentadiene, once formed, may function as a chain brancher by dissociating into the resonantly stabilized cyclopentadienyl radical and a H atom:

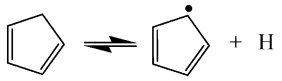

(2)

* Author to whom correspondence should be addressed. E-mail: whgreen@mit.edu.
† Massachusetts Institute of Technology.
‡ Present address: National Institute of Standards and Technology, Gaithersburg, MD 20899.
§ Colorado School of Mines.
# ExxonMobil Research and Engineering Co.

10.1021/jp0345957 CCC: $25.00
Published on Web 09/23/2003

Both the cyclopentadienyl radical and the H atom abstract H atoms from CH_4, under the experimental conditions:

(3)

The cyclopentadiene product can dissociate to cause chain branching once again. With these reactions, Dean provided the first plausible explanation for the autocatalytic upturn measured by Chen et al.[16,17]

However, recent experimental and theoretical data on the enthalpy and entropy of formation for cyclopentadienyl[20−25] indicate that reactions 1−3 alone are not sufficient to explain autocatalytic behavior.[26] Dean used a cyclopentadienyl enthalpy of formation that was similar to the value McMillen and Golden determined in 1982 ($\Delta H_f^{298} = 58$ kcal/mol),[27] whereas more-recent values from various research groups are ∼4 kcal/mol higher (clustered at ∼62 kcal/mol). With the higher enthalpy of formation for cyclopentadienyl, the dissociation barrier for reaction 2 must increase by approximately the same amount, to maintain thermodynamic consistency (reducing the rate by a factor of ∼7 at 1000 K). At this new rate, reaction 2 no longer proceeds rapidly enough to drive autocatalysis to the extent observed. Figure 1 below shows how the predictions of Dean's 1990 mechanism change when more-recent data for the cyclopentadienyl radical are used. That mechanism is now clearly unable to explain the strong autocatalysis in methane pyrolysis, and a new mechanism is needed.

1.2. Pressure Dependence and Automated Mechanism Generation. The inability to construct an accurate mechanism for methane pyrolysis by hand, in over 25 years of research, motivates our use of a computerized, automated mechanism generator to *systematically* construct a chemical model for these conditions. Such a tool must explore and include all possible "important" reactions while excluding unimportant pathways. It must also treat pressure dependence correctly, because chemical activation and falloff are crucial to methane pyrolysis (as well as many other interesting systems). But, until now, no automated mechanism generator has ever incorporated pressure dependence in an unbiased and systematic manner, despite the large number of these programs developed over the past three decades (see ref 28 for a recent review).

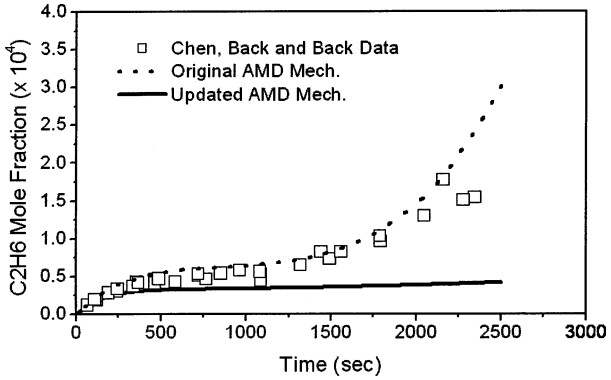

Figure 1. Attempts to explain autocatalysis in methane pyrolysis at 1038 K and 0.58 atm for very low conversions of methane. Open symbols represents experimental data sets from Chen et al. Dotted line represents the prediction of the mechanism of Dean in 1990. Solid line illustrates the Dean mechanism once again, but this time with updated kinetic parameters, most importantly improved thermodynamic data for cyclopentadienyl radical.[25] Clearly, a new model is needed to explain the autocatalysis.

Indeed, an earlier attempt by several of the co-authors to apply mechanism generation to methane pyrolysis failed to identify many of the important reactions detailed below, primarily because the approach to pressure-dependent reactions was not systematic.[29] In that approach, the rate constants $k(T,P)$ for every kinetically significant pressure-dependent reaction must be placed in a user-constructed library *before* the mechanism is generated, and only reactions appearing in this library can be included in the mechanism. But it is impossible to know which reactions will be kinetically significant before building the mechanism, and it is quite likely that even with a large $k(T,P)$ library, important pressure-dependent pathways will be omitted. Because that algorithm could not compute pressure-dependent reactions "from scratch", it essentially reproduced the 1990 Dean mechanism, which had been used as the source of its $k(T,P)$ library. The other published mechanism-generation algorithms have similar deficiencies, because they, too, cannot compute $k(T,P)$ estimates. Most of them neglect pressure dependence entirely.

Here we present the first mechanism-generation algorithm to include pressure-dependent reactions in a general and systematic manner, including on-the-fly calculations of $k(T,P)$ wherever necessary. We apply this tool, called "XMG-PDep",[30] to construct a more complete model of autocatalysis in methane pyrolysis under the conditions of Chen, Back, and Back.[15−17] The approach reveals new and unexpected pathways that can explain the autocatalytic behavior observed experimentally. Some of these pathways have never been considered in previous methane pyrolysis work and are rarely, if ever, given consideration in larger combustion or pyrolysis mechanisms.

2. Computational Method: Mechanism Generation with Integrated Pressure Dependence

XMG-PDep is based on XMG,[29,31] which was developed from NetGen,[32−35] but XMG-PDep integrates the Activated Species Algorithm for building and truncating pressure-dependent reaction networks.[36,37] A complete description of the integrated algorithm is presented in ref 30. Here we describe those features of our approach for including pressure dependence in mechanism generation which are not discussed in refs 36 and 37.

2.1. Building Pressure-Dependent Networks during Mechanism Generation. XMG-PDep considers every reaction of the form A + B → C, B → C, or B → C + D to initiate a partial pressure-dependent reaction network, such as those described in ref 37. During mechanism generation, XMG-PDep builds a set of these partial pressure-dependent networks, and from these, it constructs net pressure-dependent reactions and estimates their rate constants $k(T,P)$. Unlike the earlier work, these networks are not fully explored and then truncated to determine the important fraction necessary for $k(T,P)$ prediction.[36] Instead, each partial pressure-dependent network is explored by only one activated isomer at a time. XMG-PDep continually evaluates a "leakage" flux $R_{\mathrm{leak}(i)}$ for each partial network i. This value represents the flux to all parts of the network not yet explored; $R_{\mathrm{leak}(i)}$ decreases as activated isomers are explored and added to the network.

2.2. Determining Which Species or Isomer to Add. XMG-PDep periodically constructs a set of ordinary differential equations (ODEs) representing the evolution of the system described by its current mechanism. The code uses DASSL[38] to integrate the ODEs. At each DASSL time step, it calculates the flux $R_{\mathrm{species}(j)}$ to each candidate species that it has not yet included in the mechanism; j runs across all candidates for

inclusion. It also evaluates each leakage flux $R_{leak(i)}$, where i runs across all partial pressure-dependent networks (see refs 30 and 37).

XMG-PDep tests these fluxes against the termination criteria R_{min},

$$R_{min}(t) = f_{min}R_{char}(t) \quad (4)$$

where $R_{char}(t)$ is the characteristic rate for the entire mechanism at time t, as given by Song et al.,[39]

$$R_{char}(t) = \sqrt{\sum_k (R_{reacted(k)}(t))^2} \quad (5)$$

and f_{min} is a user-specified tolerance, typically 0.1%−1%. In eq 5, $R_{reacted(k)}(t)$ represents the net rate of change of each species already in the mechanism. If all the fluxes $R_{species(j)}$ and $R_{leak(i)}$ are less than R_{min}, integration proceeds to the next DASSL time step. If not, XMG-PDep identifies the maximum flux from the set of $R_{species(j)}$ and $R_{leak(i)}$.

When that maximum flux belongs to a candidate species (i.e., $R_{species(j)}$), XMG-PDep adds that species to the mechanism and explores its reactions with other species already included in the mechanism.[35] When the maximum flux is the leakage flux from a partial pressure-dependent network, then that network is augmented by one more isomer (or "well"), with all its pathways and channels. A new $k(T,P)$ is calculated for each reaction in that network (see refs 36 and 37). In either case, the ODE system has changed and the integration must start again at $t = 0$. When all the fluxes $R_{species(j)}$ and $R_{leak(i)}$ are less than $R_{min}(t)$ for all t from $t = 0$ to $t = t_{final}$, mechanism generation is complete, and XMG-PDep writes out a CHEMKIN version of the mechanism.

2.3. On-Line Estimation of Pressure-Dependent Rate Constants. Every time a partial pressure-dependent network is created or expanded, XMG-PDep must quickly estimate $k(T,P)$ for all of that network's pressure-dependent reactions. If the $k(T,P)$ for a specific reaction is available in a library, it will be used. But almost always, $k(T,P)$ must be calculated. To do this, XMG-PDep uses a heavily modified and accelerated version of the CHEMDIS program[40] (see ref 30 for modifications to the original code).

CHEMDIS is a Quantum-Rice-Ramsperger-Kassel/modified strong collision (QRRK/MSC) code for estimating the $k(T,P)$ of pressure-dependent reactions, given only the high-pressure-limit rate constants $k^\infty(T)$ for each elementary step in a pressure-dependent network (of arbitrary complexity), and some energy-transfer properties of the bath gas. The required density of states are estimated from the heat capacities,[41] and those, in turn, usually come from group additivity. The bath gas properties $[M]$ (the concentration of the bath gases) and $\langle \Delta E \rangle_{down}$ (the average downward collisional energy transfer) are estimated and are assumed to be unchanged over the timespan of the simulation.

CHEMDIS is a highly approximate method. While its accuracy has never been systematically studied, a substantial body of practical evidence from combustion and pyrolysis cases[36,40,42−49] suggests that the errors introduced by the QRRK/MSC approximations are acceptable for most reactions (they are usually less than the uncertainties in the $k^\infty(T)$ used as inputs). We tested the accuracy of the CHEMDIS method, under the conditions of Chen et al. (1038 K and 0.58 atm CH_4), against that of experiments or higher-level calculations for many of this work's important systems. CHEMDIS predictions were compared with measured data for the allene−propyne−cyclopropene system cited by Davis,[50] the propargyl + acetylene results of Moskaleva and Lin,[51] and all the Troe-form reactions of the rate-constant library given in the Supporting Information (the library, or literature, values were used for all these systems in the actual generated mechanism). In all these cases the CHEMDIS results were within a factor of 10 of the higher-level calculations or the experimental results, and were usually within a factor of 5. Note that the required computational intensity, and the need for detailed transition-state information for every elementary step in each pressure-dependent system, make more accurate methods (such as an RRKM/master equation approach) impractical for on-line $k(T,P)$ predictions, as we have discussed at length.[30,36,52]

3. Application to Methane Pyrolysis

We modeled the Chen, Back, and Back experiments by assuming a homogeneous, constant-volume, isothermal batch pyrolysis, starting with pure methane at the conditions they specified.[15,17] Given the small conversions and slow process evolution, as well as experimental work showing that surface reactions were not significant at the low experimental conversions,[17] the aforementioned batch model for the experiments seemed appropriate. In addition, we assumed that the pressure did not change significantly during the experiment, considering the extremely low conversion (<1%) of methane.

3.1. Initial Input Data. Generation began with an input file that specified the temperature (T = 1038 K), pressure (P = 0.58 atm), and starting mole fraction of methane ($x_{0,CH_4} = 1.0$). We used a tolerance of $f_{min} = 0.01$ and specified a final conversion of methane $X_{F,CH_4} = 0.0055$, or 0.55% methane conversion, to build a model covering the time scale of the experiments by Chen et al.

3.2. Reaction Families. XMG-PDep must use reaction families to discover elementary reaction steps. Each family has an associated reaction matrix by which graph-theory algebra is applied to produce new species and specific reactions using the methods of Broadbelt et al.[32−34] The reaction families allowed in this work, with example instances, are given in Table 1. Elementary-step families in Table 1 of the form A + B → C, C → A + B, and C → D are also used to generate the pressure-dependent pathways in each pressure-dependent network.

3.2.1. Prohibited or Nonincluded Families. We omitted certain known chemistry from Table 1 for a combination of practical and scientific reasons. First, XMG-PDep is similar to its predecessors XMG and NetGen, in that it cannot handle diradical reactions; therefore, no families that involve them can appear in Table 1. Second, failures of the on-line group contribution tool GAPP[29,31] in predicting the thermodynamic properties of a species were repaired manually using the THERM code.[53,54] However, allowing 1,3 and 1,4 intraradical additions generated a large number of strained unsaturated cyclic radicals: these confused the group-contribution tool so often that is was impossible to correct the erroneous thermochemical results manually (the group-contribution tool has recently been improved in response to these issues). Given this difficulty, and the fact that the expected barriers for these types of reactions are high and, thus, not likely to be important in the larger mechanism, 1,3 and 1,4 radical additions were left out of Table 1. Finally, similar issues, and the lack of rate estimates, made it impractical to include the *ene* reaction, Diels−Alder reactions, singlet methylenes and vinylidenes, and photochemistry, none of which are expected to be important under the conditions of

TABLE 1: Elementary-Step Reaction Families for Methane Pyrolysis Mechanism Generation at Lower Temperatures and Low Conversion of Methane[a]

FAMILY	DESCRIPTION	EXAMPLE
Dissociation	C-C and C-H bond dissociation of a molecule	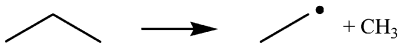
Recombination	Reverse of Dissociation	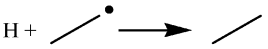
Radical Addition	Radical addition to double or triple bond of a molecule	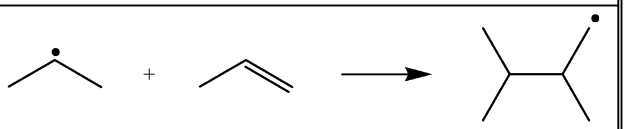
Beta-scission	Reverse of Radical Addition	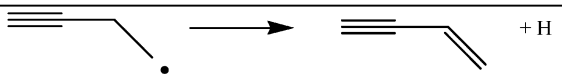
H-abstraction	Abstraction of H atom from a molecule by a radical	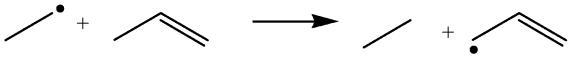
Disproportionation	Radical disprop. to form two molecules	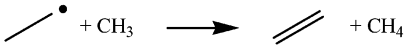
Reverse Disproportionation	H transfer to an unsaturated carbon	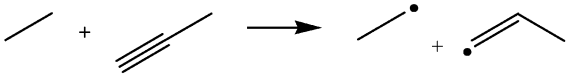
H-shift (1,2 through 1,6)	Intra-radical H-abstraction	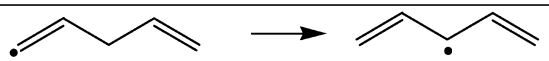
Intra-radical Addition (1,5 and 1,6)	Intra-radical addition to a double or triple bond (1,5 and 1,6 only)	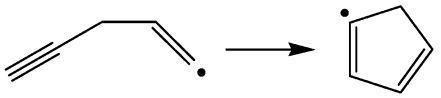
Ring-Opening Beta-scission	Beta scission which opens a ring radical (reverse of Intra-radical addition)	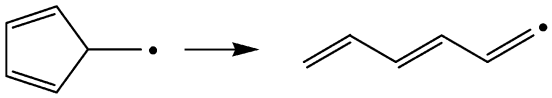

[a] These families represent all the elementary reaction types used to generate the mechanism. After a species or pressure-dependent isomer has been chosen for exploration, the generator will explore all possible instances of each family in which that species might participate.

Chen et al. It is doubtful whether any computer program will ever exhaustively include all possible reactions.

Such decisions represent a bias in our mechanism construction approach. The advantage here is that the bias is clearly defined and easily stated. Mechanism construction proceeds in a very systematic manner, given these rules. The accuracy of the generated mechanism is partially dependent on the assumption that Table 1 includes all the important reaction families at the conditions of Chen et al.

3.2.2. Allene−Propyne Isomerization. Although XMG-PDep could not build or discover reactions through diradical intermediates, the well-known allene−propyne isomerization system was included in the mechanism, because the barriers for isomerization are lower than those for dissociation to propargyl and a H atom (see, for example, refs 50 and 55), and the overall methane pyrolysis kinetics are predicted to be sensitive to allene, propyne, and propargyl. Allene may isomerize to cyclopropene, which, in turn, will rapidly isomerize back to allene or propyne, all at rates much faster than the dissociation to propargyl and a H atom. We assumed that cyclopropene formed in this system would immediately isomerize to allene or propyne, and, thus, we added three net pressure-dependent reactions directly to the reaction mechanism at the *start* of generation:

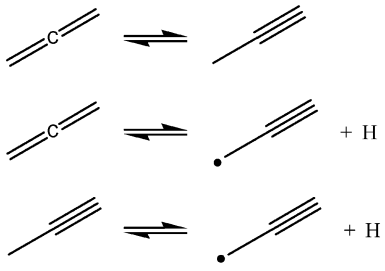

The Supporting Information gives a more complete description of our modeling of the allene−propyne isomerization system.

3.3. Thermodynamic Library. Thermodynamic parameters for 38 species were adapted in part, or wholly, from the literature; these are detailed in the Supporting Information. Different from prior work,[19,29] we use the modern values for the cyclopentadienyl radical.

Often, only a few values, such as the enthalpy of formation, could be found for a species. In these cases, we used the THERM code[53,54] to combine available literature values with group-additivity predictions to build a NASA polynomial

TABLE 2: High-Pressure-Limit Rate Rules Used in Constructing the Partial Pressure-Dependent Networks[a]

rate rule	A^∞	n^∞	E_a	source
	Recombination			
H recombination with any radical	1.00×10^{14}	0	0	ref 56
CH_3 recombination with any radical	1.00×10^{13}	0	0	ref 56
all other radical recombinations	8.00×10^{12}	0	0	ref 56
	Radical Addition			
H addition to terminal C of a double bond	1.00×10^{13}	0	1.2	ref 56
H addition to internal C of a double bond	1.00×10^{13}	0	2.9	ref 56
H addition to terminal C of a triple bond	1.70×10^{11}	0.97	2.8	ref 50[b]
H addition to internal C of a triple bond	2.03×10^{11}	0.77	6.75	ref 50[b]
CH_3 addition to terminal C of a double bond	8.50×10^{10}	0	7.8	ref 56
CH_3 addition to internal C of a double bond	8.50×10^{10}	0	10.6	ref 56
CH_3 addition to terminal C of a triple bond	1.50×10^{7}	1.87	8.2	ref 50[b]
CH_3 addition to internal C of a triple bond	8.50×10^{10}	0	10.6	ref 56
generic radical addition to terminal C	8.50×10^{10}	0	7.8	ref 56[b]
generic radical addition to internal C	8.50×10^{10}	0	10.6	ref 56[b]
	1,2 H-Shift[c]			
v → a	3.56×10^{10}	0.88	38.7	ref 57
p → p	3.56×10^{10}	0.88	40.0	ref 36
p → s	3.56×10^{10}	0.88	37.3	ref 36
p → t	3.56×10^{10}	0.88	34.6	ref 36
p → a	3.56×10^{10}	0.88	29.6	ref 36
s → s	3.56×10^{10}	0.88	39.1	ref 36
s → t	3.56×10^{10}	0.88	37.7	ref 36
s → a	3.56×10^{10}	0.88	31.5	ref 36
t → t	3.56×10^{10}	0.88	40.0	ref 36
	1,3 H-Shift[c]			
v → a	3.80×10^{10}	0.67	38.7	ref 36
p → p	3.80×10^{10}	0.67	38.8	ref 36
p → s	3.80×10^{10}	0.67	36.6	ref 36
p → t	3.80×10^{10}	0.67	34.3	ref 36
s → s	3.80×10^{10}	0.67	38.2	ref 36
s → t	3.80×10^{10}	0.67	36.1	ref 36
t → t	3.80×10^{10}	0.67	36.6	ref 36
	1,4 H-Shift[c]			
p → p	7.85×10^{11}	−0.12	23.1	ref 36
p → s	7.85×10^{11}	−0.12	20.6	ref 36
p → t	7.85×10^{11}	−0.12	18.3	ref 36
p → a	7.85×10^{11}	−0.12	15.3	ref 36
s → s	7.85×10^{11}	−0.12	23.5	ref 36
s → t	7.85×10^{11}	−0.12	20.6	ref 36
t → t	7.85×10^{11}	−0.12	19.4	ref 36
	1,5 H-Shift[c]			
p → p	3.67×10^{12}	−0.6	15.3	ref 36
	1,6 H-Shift[c]			
p → p	2.80×10^{10}	0	20.3	ref 36
	1,5 Intraradical Addition			
endo ring closure	1.22×10^{8}	1.05	15.82	ref 36
exo ring closure	2.51×10^{10}	0	6.85	ref 36
strained endo ring closure	1.22×10^{8}	1.05	17.42	see text
strained exo ring closure	2.51×10^{10}	0	8.05	see text
	1,6 Intraradical Addition			
endo ring closure	1.00×10^{8}	0.855	5.9	ref 36
strained endo ring closure	1.00×10^{8}	0.855	7.5	see text
allylic radical ring-closure correction			15	see text

[a] Values are given in units of kcal/mol and cm^3 $(mol\ s)^{-1}$ K^{-n}, using the modified Arrhenius form $AT^n \exp[-E/(RT)]$. [b] Indicates a rate rule we developed using RRHO transition-state theory and the quantum ab initio results of the reference. [c] Abbreviations in H-shifts are as follows: v, vinylic; p, primary; s, secondary; t, tertiary; and a, allylic. Nonspecific H-shift rules are given in the text and in Table 3.

representation of the thermodynamic data. All other species were estimated via GAPP or, in cases of on-line GAPP failure, using the THERM code.

3.4. Rate-Constant Library. Although XMG-PDep must usually resort to rate rules to estimate rate constants for the reactions it discovers, reliable literature data are preferable, where available. This condition is especially true for important or sensitive reactions of the mechanism. In the present example, 49 rate constants were taken from the literature; these are detailed in the Supporting Information. All the thousands of other rate constants used to construct the full model were computed on-the-fly in the present work. For some reactions, both high-pressure-limit and pressure-dependent rate constant data were available, but the pressure-dependent rate constants were not appropriate for our conditions. In these cases only the high-pressure-limit data could be used.

We performed one set of ab initio calculations to estimate the barrier and transition-state properties for the ring-opening beta-scission of 1,3-cyclopentadien-2-yl. The Supporting Information presents details of that calculation. All the reactions in

TABLE 3: General H-Shift Parameters[a]

Rotor Loss A and Parameter n[b]

number of rotors lost in TS	A^∞	n^∞
1	3.56×10^{10}	0.88
2	3.80×10^{10}	0.67
3	7.85×10^{11}	−0.12
4	3.67×10^{12}	−0.6
5	2.80×10^{10}	0.0

Ring-Strain Corrections, E_{rs}[c]

ring size	E_a
3	25.6
4	24.1
5	8.8
6	1.0
7	5.0

Evans−Polanyi	a	b
	13.4	0.6

[a] Units are the same as those presented for Table 2. These rate rules (specifically for H-shifts) are derived from Table 2 in Matheu et al.,[36] and the zero-rotor-loss case was assumed to be equivalent to the one-rotor-loss case. [b] Rotor loss (A) and n are chosen according to XMG-PDep's estimate of how many rotors are lost in going from the reactant to the transition state. [c] Ring strain E_{rs} for use in eq 6 is chosen according to how many members are in the transition-state ring for the intraradical H-abstraction.

the rate-constant library are posed in only one direction; the mechanism generator fits modified Arrhenius parameters for the reverse instance of the reaction[29] (see Chapter 6 in ref 30) to maintain the thermodynamic consistency of the mechanism.

3.5. High-Pressure-Limit Rate Rules. Tables 2 and 3 present high-pressure-limit rate rules used in the CHEMDIS calculations; Table 4 presents the rate rules for pressure-independent reactions. These rate rules were developed from a variety of sources. When the rate rules were taken from the literature, these tables give the source; in other cases, these rules were estimated based on our experience with calculations and specific literature values for instances of the reaction. Although these rate rules are modified Arrhenius parameter sets, the activation energies given have real significance: They are estimates of the true barriers for reaction and, thus, are appropriate as inputs to the pressure-dependence code CHEMDIS. All rate rules are posed in only one direction: the "designated forward" direction. The mechanism generator fits modified Arrhenius parameters for the reverse instance of the reaction, which were computed using the thermochemistry.

3.5.1. H-Shifts. The "specific" H-shifts in Table 2 are used for the specified unimolecular transformation from the radical of the first type to the radical of the second type. For example, the "1-2 H-Shift, p → s" is a rate rule for a unimolecular H-shift reaction that converts a primary radical to a secondary radical. Table 3 represents parameters used to evaluate *general* H-shifts, i.e., the default if no value for a specific type is available. In these cases, A^∞ and n^∞ were selected from the rotor loss A^∞ and n^∞ values in Table 3, as described in Matheu et al.[36] The generator then evaluates the barrier height E_a, via the relation

$$E_a^\infty \approx E_{rs} + a + b\Delta H_{rxn}^{298} \qquad (6)$$

where E_{rs} is the appropriate ring-strain correction and a and b are Evans−Polanyi parameters, all chosen from Table 3. For endothermic H-shifts, the rate for the exothermic direction would be estimated and converted to the desired direction, using the reaction thermochemistry, followed by the reverse Arrhenius parameter fitting procedure mentioned previously.

3.5.2. Intraradical Ring Closures. Rate rules for intraradical ring closures are first divided into "exo" and "endo" forms. In exo-ring closures, the radical site adds to the unsaturated bond in such a way that the product radical site is not on the formed ring. In endo-closures, the radical site ends up on the formed ring. These are further divided into strained and unstrained ring closures. On the basis of the work of Moskaleva and Lin,[51] a correction of 1.6 kcal/mol was added to the barrier for cases where the transition state for the ring closure would be "strained"; that is, it would have two consecutive partial double bonds, or a partial triple bond, in the transition state.

Finally, considering the work of Martinez and Cooksy[58] and our B3LYP/6-311G** calculation for the ring-opening transition state of 1,3-cyclopentadien-2-yl (see the Supporting Information), we added 15 kcal/mol to any ring closure that starts from an allylic-stabilized reactant. Such reactants must give up their allylic stabilization to undergo ring closure; the 15 kcal/mol penalty used above is approximately the difference between

TABLE 4: Rate Rules for Non-Pressure-Dependent Reactions[a]

rate rule	A	n	E_a	source
H abstraction by H (generic)	4.55×10^6	2.0	5.0	ref 56
H abstraction by H to form a primary radical	9.33×10^6	2.0	7.7	ref 56
H abstraction by H to form a secondary radical	4.55×10^6	2.0	5.0	ref 56
H abstraction by H to form a tertiary radical	1.26×10^{14}	0	7.3	ref 56
H abstraction by CH_3 (generic)	2.00×10^{11}	0	9.5	ref 56
H abstraction by CH_3 to form a primary radical	2.17×10^{11}	0	11.6	ref 56
H abstraction by CH_3 to form a secondary radical	2.00×10^{11}	0	9.5	ref 56
H abstraction by CH_3 to form a tertiary radical	1.00×10^{11}	0	7.9	ref 56
H abstraction by C_2H_5 (generic)	2.50×10^{10}	0	10.4	ref 56
H abstraction by C_2H_5 to form a primary radical	1.67×10^{10}	0	13.4	ref 56
H abstraction by C_2H_5 to form a secondary radical	2.50×10^{10}	0	10.4	ref 56
H abstraction by C_2H_5 to form a tertiary radical	1.00×10^{11}	0	7.9	ref 56
H abstraction by C_2H_3 (generic)	1.02×10^3	3.1	8.8	from $C_2H_3 + C_3H_8$ to *i*-C_3H_7 in ref 59
H abstraction by C_2H_3 to form a primary radical	6.02×10^2	3.3	10.5	from $C_2H_3 + C_3H_8$ to *n*-C_3H_7 in ref 59
H abstraction by C_2H_3 to form a secondary radical	1.02×10^3	3.1	8.8	from $C_2H_3 + C_3H_8$ to *i*-C_3H_7 in ref 59
H abstraction by C_2H_3 to form a tertiary radical	9.03×10^{-1}	3.5	2.61	from C_2H_3 + *i*-C_4H_{10} to *tert*-butyl in ref 60
H abstraction by any radical	2.50×10^{10}	0	10.4	from that previously given for "H abstraction by C_2H_5"
H abstraction by any radical to form a primary radical	1.67×10^{10}	0	13.4	from that previously given for C_2H_5
H abstraction by any radical to form a secondary radical	2.50×10^{10}	0	10.4	from that previously given for C_2H_5
H abstraction by any radical to form a tertiary radical	1.00×10^{11}	0	7.9	from that previously given for C_2H_5
disproportionation (all)	1.00×10^{12}	0	0	ref 61

[a] Units are the same as those given in other tables (kcal/mol, cm^3 (mol s K)$^{-1}$).

the barrier for 1,3-pentadien-5-yl ring closure as predicted by Martinez and Cooksy and the barrier from the normal 1,5 endo-ring-closure rule.

3.6. Pressure-Independent Rate Rules. Table 4 shows the rate rules used for non-pressure-dependent reactions in this work. These rate rules are taken from various sources.

3.7. Other Data. Table 2 in the work by Dean, Bozzelli, and Ritter[42] provided Lennard-Jones parameters and $\langle\Delta E\rangle_{all}$ for methane as a bath gas; from their value of $\langle\Delta E\rangle_{all}$, we estimated $\langle\Delta E\rangle_{down} = 1285\ cm^{-1}$ at 1038 K. Lennard-Jones collision parameters for most other species were provided by GAPP, or by default values, on the basis of the number of heavy atoms and whether the species was cyclic. Generally, the CHEMDIS calculations were not very sensitive to the Lennard-Jones values used.

4. Results: The Methane Pyrolysis Mechanism

XMG-PDep examined over 12 000 candidate species and 12 000 possible pressure-dependent networks as it automatically constructed a methane pyrolysis mechanism for the Chen, Back, and Back experiments. The code performed more than 300 on-the-fly $k(T,P)$ estimations via CHEMDIS. The final generated mechanism has ~100 species and ~1000 reversible reactions, 342 of which are pressure-dependent; it may be the first accurate mechanism developed systematically via flux-limit criteria. No attempt has been made to reduce or condense the mechanism. No parameters were adjusted to fit the data.

Of the 12 000 possible pressure-dependent networks examined, <400 could be considered "active" (that is, networks for which at least one $k(T,P)$ calculation was required). In all the other possible networks, XMG-PDep found that the value of $R_{leak(i)}$ did not justify expansion of the network beyond the entrance channel. These inactive cases were all chemical activation systems in which $R_{leak(i)}$ was equal to the entrance channel's estimated reactant concentrations multiplied by $k^{\infty}(T)$. Even with this value (which is the highest possible for $R_{leak(i)}$ in a given network), $R_{leak(i)}$ was still less than R_{min} for the entire simulation, and so these networks never needed exploration.

The Supporting Information presents this mechanism in CHEMKIN format. A record of each active pressure-dependent network, with sufficient information to build the CHEMDIS input file and to estimate $k(T,P)$, is also included.

Figure 2 highlights the ability of the computer-generated mechanism to predict autocatalysis. Our prediction for the ethane mole fraction agrees well with the data of Chen, Back, and Back from various experiments. The computer-generated mechanism prediction does miss the ethane plateau concentration, by ~35%, but falls within the error of repeated runs in the autocatalytic regime ($t > 2000$ s).

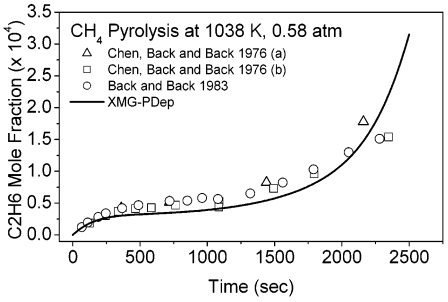

Figure 2. XMG-PDep generated mechanism prediction for ethane concentration versus time, compared with various experimental data sets.[15,17] Data set (a) refers to the data table of ref 17; data set (b) refers to data from Figure 4 of the same work. The generated model predicts the autocatalysis without recourse to parameter adjustment or fitting.

In addition to ethane, the principal stable products of methane pyrolysis under these conditions and at low conversion are hydrogen, ethylene, acetylene, propene, allene, and propyne; of these products, Back and co-workers measured all but propyne. Figures 3−7 show how the mechanism agrees with measured concentrations of these species. Predictions for acetylene and propene concentrations, in particular, are much improved over the 1990 Dean mechanism.[19]

The last plot (Figure 7) shows some discrepancy between the measured and predicted concentrations of allene at later times; this is addressed in the Discussion. In all other cases, agreement of the unadjusted, unfitted mechanism with the data is quite good. Thus, our pressure-dependent mechanism-generation algorithm succeeds in capturing the vital elements

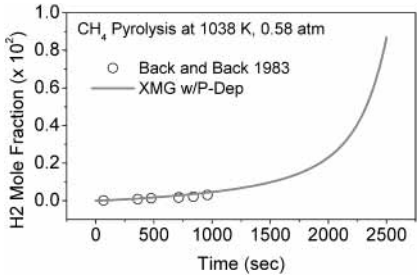

Figure 3. XMG-PDep predicted hydrogen mole fraction versus experimental data.

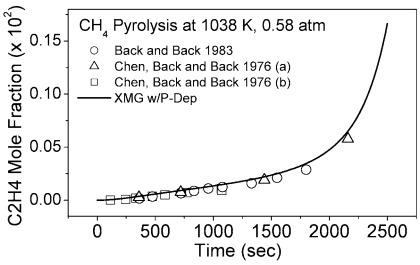

Figure 4. XMG-PDep predicted ethylene mole fraction versus experimental data.

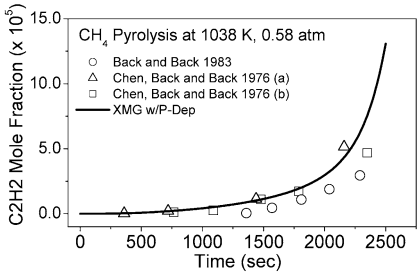

Figure 5. Acetylene mole fraction prediction versus experimental data. Compare this graph to Figure 4 in the work of Dean[19] and note the improvement in the prediction of this important species.

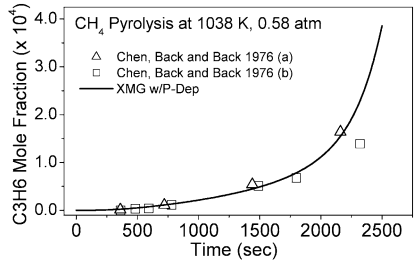

Figure 6. Propene mole fraction prediction versus experimental data.

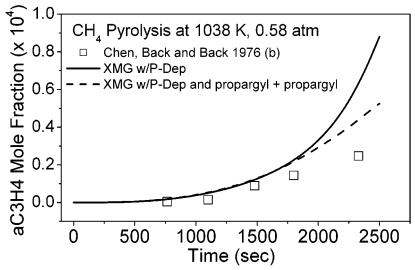

Figure 7. Allene mole fraction prediction versus time, compared with experimental data. Dotted line shows the effect of including our best by-hand model of the complicated propargyl + propargyl system.

of methane pyrolysis under these conditions, with no fitting or adjustment of *any* parameters to the experimental data.

5. Discussion

5.1. Sources of Autocatalysis. Sensitivity and rate-of-production/destruction analyses alone are not sufficient to show what leads to autocatalysis in the new mechanism. A radical-production analysis is needed to learn which reactions provide the greatest net increase in radicals and are therefore the "most" chain-branching. Combining radical production, sensitivity, and rate-of-production/consumption provides a comprehensive picture of pathways in methane pyrolysis.

5.1.1. Radical Production Analysis. The top three net-radical-producing reactions, along with selected other reactions, are shown in Figure 8, with their net production rates as a function of time. Cyclopentadiene is still important as a chain brancher, but reverse disproportionations are also quite important for radical production. In particular, the reverse disproportionation of allene and methane to form an allyl radical plus a methyl radical seems to be crucial during the induction period.

5.1.1.1. A Key Route to Cyclopentadienyl. As noted previously, with modern thermochemistry, the allyl + acetylene channel (reaction 1) does not produce sufficient cyclopentadiene to account for autocatalysis. The mechanism generator found a different chemically activated pathway, one that produces the cyclopentadienyl radical directly (in the Supporting Information, see pressure-dependent network 158):

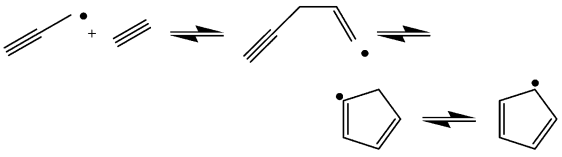

(7)

The net pressure-dependent reaction propargyl + acetylene → cyclopentadienyl accounts for almost all the net cyclopentadienyl radical production in our system. The cyclopentadienyl then abstracts H atoms from CH_4 to form a cyclopentadiene that dissociates relatively quickly, in a chain-branching reaction. To our knowledge, no previous methane pyrolysis mechanism included the propargyl + acetylene pathway. Note that, without integrated pressure dependence, our mechanism generator could not have discovered this important reaction system.

At first, the ring-closure step in reaction 7 might seem too strained to be reasonable. Moskaleva and Lin recently performed a detailed computational study of the potential surface for the cyclopentadienyl dissociation system, which included the propargyl + acetylene channel.[51] They found the barrier for the ring closure to be only slightly more than that for an unstrained ring closure, such as that forming cyclopentyl.[36] In addition, Knyazev and Slagle[62] found strong experimental evidence for a C_5H_5 product from propargyl addition to acetylene. Its thermal stability, and experimental agreement with the prediction of Moskaleva and Lin, suggest that this species is cyclopentadienyl formed via the chemically activated pathway of reaction 7. Thus, cyclopentadienyl formation via propargyl + acetylene is quite reasonable and should be expected under our methane pyrolysis conditions.

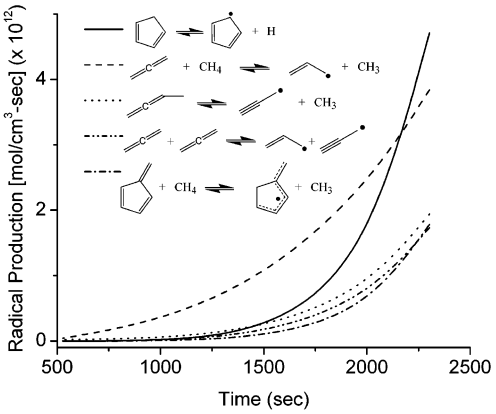

Figure 8. Main radical production routes for autocatalysis in methane pyrolysis. Each curve represents a *net* rate, in which the reverse recombination or disproportionation flux has been taken into account. Note the early importance of the allene + methane pathway. There are four other pathways with curves very similar to that for fulvene + methane; these have been left out for clarity.

The allyl + acetylene channel, previously proposed as a route to the cyclopentadiene/cyclopentadienyl chain branching, seems to be unimportant, under these conditions. With our tolerances, XMG-PDep does not explore this pressure-dependent network beyond the first adduct. The addition of the full allyl + acetylene pressure-dependent network, by hand, to the generated mechanism produces very little change in any of the species profiles. This result might seem strange at first, because the initial barrier for propargyl addition to acetylene is higher than that for allyl addition to acetylene. However, our rate constants for the pressure-dependent reactions

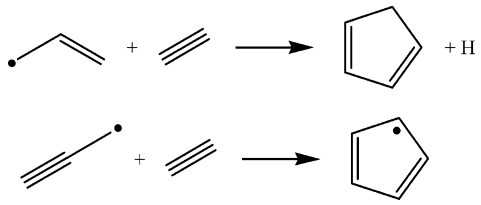

are quite similar ($\sim 1.0 \times 10^9$ cm^3 (mol s)$^{-1}$ at 1038 K and 0.58 atm methane), because of the particular structure of their corresponding pressure-dependent networks. Furthermore, both the Dean mechanism and the generated mechanism agree that the concentration of propargyl is considerably larger than that of allyl. The generated mechanism includes loss pathways for the allyl radical (specifically, H-shifts to vinylic species), which were left out of the Dean 1990 mechanism—these further lower the concentration of the allyl radical in the new simulation, making the allyl + acetylene pathway even less important.

5.1.1.2. Importance of Reverse Disproportionation Reactions. Figure 8 shows that reverse disproportionation of allene and methane to form allyl and methyl radicals is key to explaining autocatalysis in methane pyrolysis; the cyclopentadiene chain-branching reaction accounts for only 25% of radical production after 2450 s (the endpoint of model integration, where $X_{CH_4} = 0.0055$). Cumulatively, reverse disproportionations seem to be quite important and account for more than half of the radical

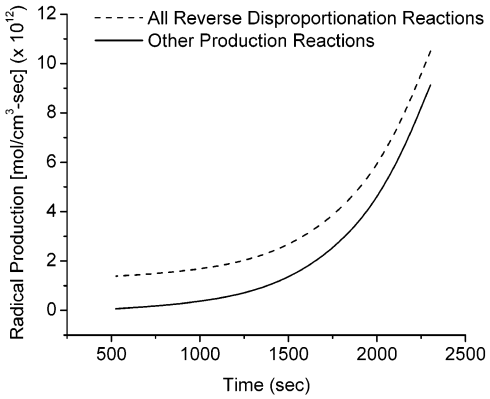

Figure 9. Total *net* radical production from all reverse disproportionation reactions, compared to radical production from all other reactions except methane dissociation, which produces radicals at a constant 1.3 $\times$ 10^{12} mol $(cm^3\ s)^{-1}$.

production during the induction period leading to the autocatalytic regime (see Figure 9).

To predict the reverse disproportionation rate constants, XMG-PDep uses thermodynamic reversibility and the single disproportionation rule in Table 4, as given by Dahm.[61] In general, disproportionation reactions are not well-studied experimentally or theoretically, but the Dahm rate rule could be considered somewhat high. Tsang's review[63] suggests a rate constant of 3.3 $\times$ 10^{11} cm^3 $(mol\ s)^{-1}$, compared to the Dahm rate rule of 1.0 $\times$ 10^{12} for the reverse of the key molecular addition:

(8)

Using Tsang's recommendation for this reaction has little effect on the predicted ethane concentration, however, lowering it by less than 15% in the autocatalytic regime. The effects on the other measured species mentioned in Figures 4−8 are similarly small.

In addition, Dahm's "fast" rate rule is within the range of disproportionation rate constants suggested by the Allara and Shaw tables;[64] these authors gave estimates in the range of 1.6 $\times$ 10^{11}−2.0 $\times$ 10^{12} cm^3 $(mol\ s)^{-1}$ per H atom for the disproportionation of small alkyl radicals with each other. Disproportionations in which the H atom is the abstractor can be higher by an order of magnitude, so it is not clear that Dahm's rule is necessarily too fast, if one is applying a general rule for all disproportionations.

Significant radical production via reverse disproportionation is not merely a consequence of the Dahm rate rule. Reducing the rate constant by a factor of 3 for the top five reverse disproportionation reactions has the effect shown in Figure 10 on predicted ethane concentration. The autocatalytic effect is still present, although it is clearly weaker with the reduced rate. Thus, while Dahm's rule may be primitive, the computer-generated mechanism suggests that, as a class, reverse disproportionations are critical to explaining the radical production that leads to methane autocatalysis at lower temperatures.

This work is the first to suggest the specific importance of reverse disproportionations to methane autocatalysis. An earlier mechanism did include a few of these reactions;[19] Back and Back suggested broadly that "bimolecular reactions of unsaturates" could contribute to autocatalysis.[15] But in other cases, no reverse disproportionations were included (see, for example, ref 18), and these reactions were once assumed to be too slow to be of importance.[17]

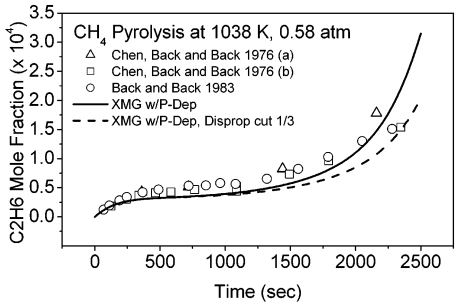

Figure 10. Predicted ethane concentration when the rate is reduced by a factor of 3 for the top five reverse disproportionation reactions. The autocatalytic effect is still pronounced and is still within the data scatter at ~2400 s. Plots for other species in this case (one-third of the disproportionation rate) show little change, or mild improvement, in terms of agreement with data.

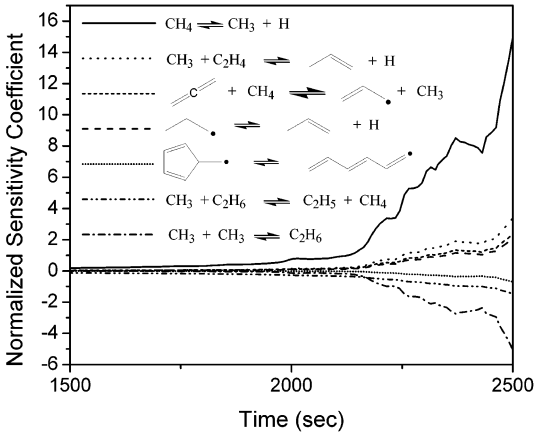

Figure 11. Normalized sensitivity coefficients for ethane formation in the autocatalysis regime. Reactions are written in the direction of net flux at 2450 s. Because the thermochemistry is fixed, increasing a rate constant forward also increases its reverse. The "noise" in the curves is a consequence of solving the sensitivity equations with a loose tolerance and is not physically significant.

5.1.2. Sensitivity and Rate-of-Production/Consumption Analysis. Normalized sensitivities from the SENKIN program[65] for ethane are presented in Figure 11. Because these sensitivities were computed using reversible reactions and fixed thermochemistry, both the forward and reverse rate constants are varied simultaneously. Since conversion of methane is quite low, methane dissociation dominates the sensitivities. Unimolecular ethane decomposition to methyl radicals has the strongest negative influence. The reverse disproportionation of methyl and allyl radical appears again in this analysis. The pressure-dependent addition of methyl radical to ethylene, to form propene and a H atom, seems to be a key step, as is the pressure-dependent beta-scission of propyl radical. In fact, of the four reactions with significant positive sensitivities, three "produce" an allyl radical or propene (the disproportionation reaction net flux is toward allyl and CH_3). This suggests that allyl or propene formation could be rate-limiting for the onset of autocatalysis, as signified by the end of the "plateau" in ethane concentration.

A relative rate-of-consumption analysis supports the idea of propene or allyl-radical formation being generally rate-limiting in the autocatalytic regime, as suggested by Figure 12. Propene and the allyl radical are entrance points to "loop" pathways with significant chain branching and methane consumption. First, more than half of the propene at 2450 s forms allyl radicals. The majority (65%) of the allyl will form propyne or allene by direct beta-scission, or by a pressure-dependent H-shift

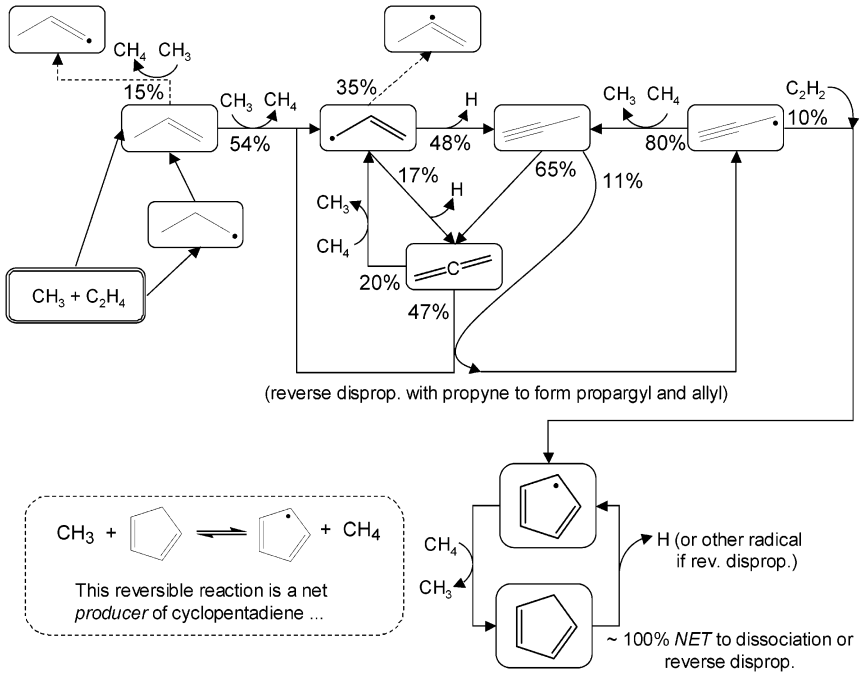

Figure 12. Important net fluxes during autocatalysis at 2450 s. Not all pathways are shown. Dotted connections are to species that can effectively re-enter the allene loop via beta-scission (to propyne or allene). Some of the propargyl formed by this loop will combine with acetylene, initiating a more powerful cyclopentadiene autocatalysis loop. While most cyclopentadiene is actually "consumed" by the methyl radical abstraction of hydrogen, the net effect of this reversible reaction is to produce cyclopentadiene from cyclopentadienyl. Note that this is *not* a steady-state picture but instead represents predicted fluxes in the autocatalytic regime.

followed by beta-scission. Propyne and allene are rapidly equilibrated via the isomerizations through cyclopropene, as studied by Davis,[50] so that propyne in excess of equilbrium quickly becomes allene.

Next, some of the allene undergoes reverse disproportionation with methane to re-form allyl radicals. This process forms radicals, so that the reaction "loop" from allyl to allene, followed by the chain-branching conversion of methane to methyl, is a powerful acceleration mechanism.

Much of the remaining allene will undergo reverse disproportionation with propyne to give a propargyl radical. In all, more than two-thirds of the allene participates in chain-branching reverse disproportionation of some type. The great majority of the propargyl abstracts hydrogen from CH_4 to re-form propyne, which is equilibrated with allene, closing the outer loop.

Finally, some of the propargyl combines with acetylene to form the cyclopentadienyl radical via reaction 7. The cyclopentadienyl loop in Figure 12 represents a second chain-branching system, because cyclopentadienyl recombination with a H atom is not significant under these conditions. Most cyclopentadienyl will abstract a H atom from methane, forming cyclopentadiene. Almost all of this cyclopentadiene eventually undergoes a chain-branching dissociation or reverse disproportionation to re-form cyclopentadienyl (the combination of reaction 3 and its reverse is actually a net cyclopentadiene producer, because of the high concentration of methane). Figure 8 would suggest that the cyclopentadienyl and allene−allyl loops are, roughly, equally important in explaining methane autocatalysis, although the relative significance of the cyclopentadienyl system grows as the methane conversion increases.

Figure 12 implies that allyl decomposition to allene and a H atom could be quite important. In XMG-PDep, the barrier for allyl radical beta-scission is calculated from the reverse of the library parameters for hydrogen addition to allene to form the allyl radical.[50] We find that increasing the barrier by 2 kcal/mol in the relevant pressure-dependent networks has only a weak affect on the predicted allene concentration and the predicted ethane concentration (as Figure 11 would imply, in that beta-scission of an allyl radical does not seem to be a sensitive reaction). A possible explanation lies in Figure 12 itself: decreased allene formation by direct allyl beta-scission simply means that more allyl radical converts to propyne, which then finds its way to allene. This explanation is only tentative, however, because the barriers for the pressure-dependent H-shift and beta-scission steps that convert the allyl radical to propyne and a H atom are also uncertain.

5.1.3. Adding Allene or Propene to Methane Pyrolysis. The comprehensive picture in Figure 12 might lead one to conclude that adding a very small amount of propene or allene to methane at the start of pyrolysis, under the conditions of Chen, Back, and Back, could have a strong effect on the results. Figure 13 shows that this is partially true. The addition of propene or allene at a very small concentration (a mole fraction of 1.0×10^{-5}) would seemingly boost the concentration of ethane in the autocatalytic regime by ~40%−50%. The addition of the same

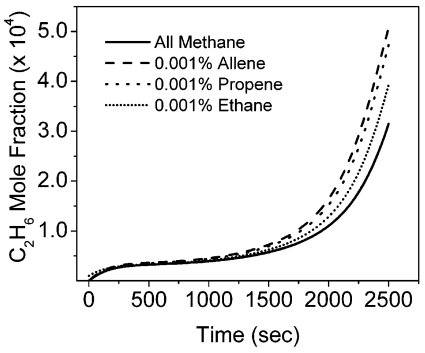

Figure 13. Predicted response of the ethane product in methane pyrolysis to the addition of very small amounts of allene, propene, or ethane at the beginning of the Chen et al. experiments. Note that the addition of almost any small amount of alkane or alkene will have a promotional effect.

amount of ethane, however, has a similar (although diminished) effect, probably because the ethane will convert to a methyl radical and/or ethylene, which, together, readily form propene. In fact, almost *any* stable alkane, alkene, or alkyne could form the ubiquitous allyl or propargyl radicals in just a few steps under these conditions, providing an alternate entry point to these radicals in Figure 12. Indeed, we find that adding any one of many stable species of the mechanism (acetylene, 1-butyne, 2-butyne, 1,2 butadiene, 1-methyl-1,3-cyclopentadiene), in a very small concentration, has an effect similar to that for propene or allene in Figure 13. Exceptions include hydrogen gas and benzene, which have no effect at the low mole fraction (1.0×10^{-5}) and the low conversions of this work. This result is expected, because hydrogen and benzene do not have facile, rapid routes to allyl or propargyl radicals in our model.

Although small, the difference between the effects of incremental amounts of ethane, benzene, and allene at least suggest simple experiments to examine whether an incremental amount of allene would have a more pronounced effect on methane pyrolysis than the same amount of ethane. Such an experiment would be a helpful test of our mechanism's accuracy.

5.2. Allene Concentration. As noted earlier, Figure 7 shows some discrepancy between the predicted and measured allene concentrations. There is only one data set for allene concentration under the conditions of Chen et al.;[17] despite many experiments and reviews on methane pyrolysis by these researchers,[15−17,66−68] the allene measurement was never repeated. This seems odd, because in Figure 4 of the work by Chen et al.,[17] allene is the only measured species that seems to plateau *after* the autocatalytic regime has set in. Such behavior should mark it as a species of interest. For various reasons, our mechanism generator was halted at the methane conversion specified above, and thus the generated mechanism could not, technically, predict whether allene would plateau after 2500 s, as the Chen, Back, and Back figure implied. However, integrating our mechanism beyond this endpoint of generation did predict a plateau in the allene concentration.

Assuming that the measured allene profile represented real behavior, we attempted to correct our model prediction by adding a version of the propargyl + propargyl pressure-dependent reaction network, as studied by Miller and Melius.[69] It is believed that, via a chemically activated, pressure-dependent network, propargyl radicals may combine to form benzene and fulvene, as well as the direct recombination isomers. Unfortunately, XMG-PDep cannot handle reactions through diradical intermediates and did not have the reaction families which would represent some of the unusual isomerizations that occur in the propargyl + propargyl network. Thus, the mechanism generator could not have found this system "on its own".

Therefore, we used hand-constructed CHEMDIS input files (provided by H.-H. Carstensen[70]) representing the head-to-head, head-to-tail, and tail-to-tail chemical activation channels for this system, based on the surface described in the work of Miller and Melius.[69] The resultant net reactions were added to the generated CHEMKIN mechanism. This lead to a marked improvement in the allene prediction, as compared with the experimental result, as Figure 7 shows.

The addition of the propargyl + propargyl system weakly affects other species concentration predictions in Figures 4−8, in the regimes where experimental data are available. The predicted ethane concentration increases by ~40% at 2400 s, putting it just above the highest data point in Figure 2; other species profiles increase by 10%−30% in the autocatalytic regime. The predicted concentration of hydrogen in Figure 3 increases by a factor of 2 at 2500 s, but no data are available in this range. Generally, the results of Figures 4−8 are not seriously perturbed and are largely unchanged in the regions where data are available. The broad effect of autocatalysis is still clearly present.

It may seem odd that allene, which is so important in Figures 11−13, could be halved in concentration, with other species profiles unchanged or somewhat increased. The likely explanation is that many species can perform the role of allene in Figure 12. In particular, fulvene (which is a key product of the propargyl + propargyl recombination) undergoes reverse disproportionation to form resonantly stabilized radicals; the importance of fulvene is already implied by Figure 11. Probably, fulvene makes up the chain-branching deficiency left by depleted allene in this hand-adjusted mechanism, so that other species concentrations remain unaffected. In any case, the mechanism is likely more accurate with the propargyl + propargyl system included.

5.3. CH_4 Pyrolysis under Other Conditions. Chen et al. examined other conditions near 1038 K and 0.58 atm, although they reported specific pressures for only a few of these experiments. We successfully applied our mechanism generator to their 1038 K/0.13 atm and 1103 K/0.59 atm cases, using the same reaction familes, rate rules, rate-constant library, and thermodynamic library as for the main example at 1038 K/0.58 atm. The mechanisms generated at these conditions are available from the authors; in both cases, the autogenerated models captured the measured species concentrations well, without adjustment of any parameters, validating the algorithmic approach and data used for the main case.

5.3.1. Conditions of 1038 K and 0.13 atm. Figures 14 and 15 respectively show predicted results from the generated mechanism for ethane and ethylene concentration against measured data at 1038 K and 0.13 atm. Agreement of the predicted concentrations with experimental data is good, comparable to that found in the pre-autocatalytic region of Figures 2 and 4 (the *y*-axis scales in Figures 14 and 15 are greatly expanded, compared to those in Figures 2 and 4, which span much-larger concentration ranges in order to show the autocatalysis at later times).

Because this experiment did not proceed to the autocatalytic regime, the mechanism generated for 1038 K and 0.13 atm turns out to be a subset of that generated at 1038 K and 0.58 atm. No new chemical pathways appear at this lower pressure. In fact, for the pre-autocatalytic region, the concentrations of the two measured species are strongly dependent on the rates of only a few reactions:

$$CH_4 \rightleftharpoons CH_3 + H$$

$$CH_3 + C_2H_6 \rightleftharpoons CH_4 + C_2H_5$$

$$CH_3 + CH_3 \rightleftharpoons C_2H_6$$

The rates and thermochemistry for these three pathways (two of which are pressure-dependent) are drawn from the reaction rate library and thermodynamic data library. Only a few reactions control behavior in the pre-autocatalytic regime; therefore, it is no surprise that the reactions found by the generator for the 0.13 atm experiment are a subset of those found for the 0.58 atm case.

5.3.2. Conditions of 1103 K and 0.59 atm. The Chen et al. experiment at 1103 K and 0.59 atm produced carbon film deposits soon after the onset of autocatalysis (after ~225 s). XMG-PDep does not treat surface chemistry; furthermore, the

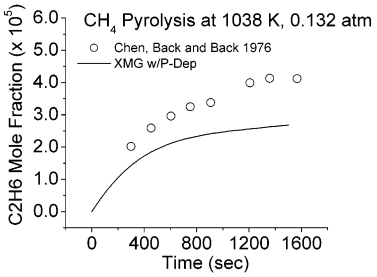

Figure 14. XMG-PDep generated mechanism prediction for ethane mole fraction versus time at 1038 K and 0.13 atm. Symbols are data from Chen et al.[17] Compare this figure with Figure 2 (1038 K and 0.58 atm) but note that the *y*-axis scale in this graph is 10 times larger than that in Figure 2; these data are in the pre-autocatalytic regime.

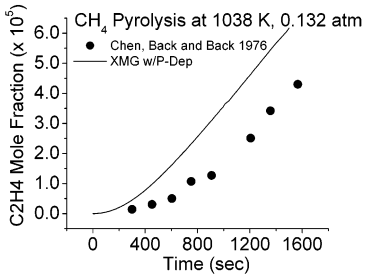

Figure 15. XMG-PDep generated mechanism prediction for ethylene mole fraction at 1038 K and 0.13 atm; symbols are data from Chen et al. Compare this figure with Figure 4 but note that the *y*-axis scale is expanded by a factor of 1000 in this figure.

sharp increase in the number of discovered species and reactions soon after the onset of autocatalysis made mechanism generation beyond 250 s prohibitive. For these reasons, we halted generation at 250 s (∼0.8% conversion of CH_4).

Figure 16 presents the generated model's predicted ethane concentration, along with experimental data at 1103 K and 0.59 atm. The generated mechanism once again captures the autocatalytic effect well, with an accuracy similar to that in Figure 2. Figures 17 and 18 respectively show our results for the ethylene and acetylene concentrations; agreement with the experiment is good, although the generated model overpredicts these species at later times.

The 1103 K/0.59 atm mechanism is very similar to that discovered for the 1038 K/0.58 atm main example. Cyclopentadiene dissociation to cyclopentadienyl and a H atom (reaction 2) is still the most important chain-branching reaction in the autocatalytic region, followed by allene and methane reverse disproportionation (reaction 8). The fulvene−allene reverse disproportionation of Figure 8 is also important at 1103 K. The generator does find a few more triple-bonded species at the higher temperature, but all the reactions important to autocatalysis appear in both mechanisms.

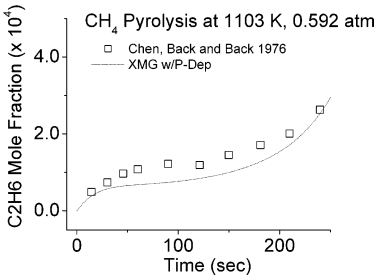

Figure 16. Predicted and experimental ethane concentration for the Chen et al. experiment at 1103 K and 0.592 atm.[17] XMG-PDep captures the autocatalytic effect under these conditions also, using the same data libraries as those used for the main example presented.

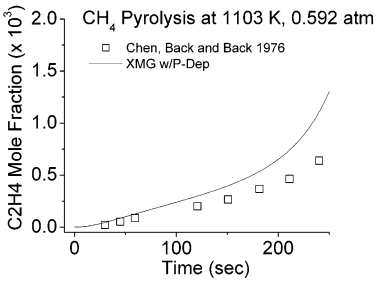

Figure 17. Predicted and experimental ethylene concentration at 1103 K and 0.592 atm.

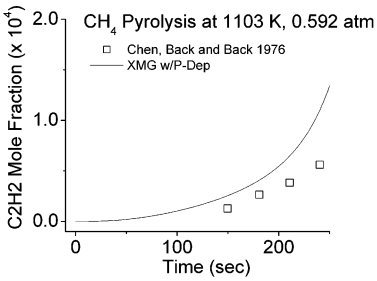

Figure 18. Predicted and experimental acetylene concentration at 1103 K and 0.592 atm.

Although the mechanisms are largely the same, dissociation reactions forming resonant stabilized radicals, such as reactions 9 and 10, seem to be more important at the higher temperature:

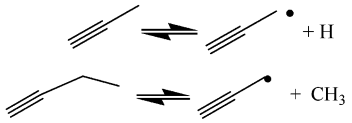

(9)

(10)

At the same time, many of the secondary reverse disproportionation pathways (examples of which are shown in Figure 8) become less significant to net radical production at 1103 K.

The 1038 K/0.13 atm and 1103 K/0.59 atm conditions are quite similar, from a chemical kinetics standpoint, to the main case studied here; thus, the success of the mechanism generator for these cases is expected. But the accurate description of nearby conditions supports the modeling and analysis of the main example at 1038 K and 0.58 atm.

5.4. Directions for Model Improvement. *5.4.1. Disproportionation and Molecular Addition.* Figures 10−12 suggest the need for more accurate disproportionation rate constants. The accuracy of the mechanism depends, in part, on the rate of methyl + allyl disproportionation and its reverse, which has not yet been successfully measured[71] (although ethyl + allyl disproportionation has been measured,[72] with the recommended rate constant being almost exactly equal to the Dahm rule[63]). Kinetic experiments and computational work in lower-temperature methane pyrolysis should consider the disproportionation of allyl and methyl radicals.

5.4.2. Missing Families and the Propargyl System. It is not reasonable to proceed further with automated mechanism development for methane pyrolysis until certain diradical-intermediate isomerization families can be added systematically; in particular, systems such as propargyl + propargyl need to be handled properly. In addition, the diradical intermediate isomerization of propyne and allene (through cyclopropene) seems possible for any triple-bonded or allenic species and should at least be considered for species such as 1,2-butadiene. Finally, *ene* reactions, concerted eliminations, 1,3 and 1,4 intraradical additions, and retro-Diels−Alder reactions are

among the families not considered in this work; extension of this mechanism may need to include such families.

6. Conclusions

6.1. Automated Mechanism Generation. This work describes the first known mechanism generation tool that can include pressure dependence in a general and systematic fashion and can compute needed rate constants $k(T,P)$ on-the-fly. The XMG-PDep tool builds a mechanism for low-temperature methane pyrolysis, from scratch, that adequately explains the autocatalytic behavior of that system. In applying it, this work is the first to apparently resolve the mystery of low-temperature methane autocatalysis while employing accurate thermodynamic parameters for the important species. Successful automated generation of the methane pyrolysis mechanism would have been impossible without an integrated pressure-dependence tool; this is a problem only a pressure-dependent mechanism generator (as opposed to other generators) could have approached.

6.2. A New Model for Lower-Temperature Methane Pyrolysis. Predicted concentration profiles from the new, computer-generated mechanism agree well with almost all measured data at 1038 K and 0.58 atm and at nearby conditions of 1038 K/0.13 atm and 1103 K/0.59 atm. The new model suggests that, initially, autocatalysis stems in large part from a set of rarely considered reverse disproportionation reactions. The cyclopentadiene/cyclopentadienyl chain-branching system cited by Dean[19] is also quite important, especially at later times, but the source of these species is actually the direct formation of cyclopentadienyl from propargyl and acetylene, not the previously proposed formation of cyclopentadiene from allyl and acetylene. Although the current model is appropriate only for a low conversion of methane at ~1038 K and 0.58 atm, any model including methane pyrolysis, operating near this regime, probably needs to account for the chain-branching loops of Figure 12.

Reverse disproportionation of allene and methane seems to be a key step, but other species could easily play the same role that allene does in this study. Experiments in which very small amounts of allene or certain other species are added to methane at the start of pyrolysis might help confirm the mechanism presented here, in that our work predicts that allene or other reactive unsaturated species will have a stronger effect than the same amount of ethane, hydrogen, or benzene.

The success of this new, computer-aided approach for accurately predicting such complex kinetics, without any adjustable parameters, is extremely encouraging. Moreover, this computer tool was able to identify critical reaction pathways missed by experienced kineticists. In the future, systematic tools such as XMG-PDep may allow kinetic modelers to build accurate, predictive models for a variety of processes, while avoiding the type of extensive parameter fitting that sacrifices understanding for agreement with data.

Acknowledgment. The authors thank Dr. R. Sumathi for providing the TST code and for performing or assisting with the ab initio calculations used in this work. Dr. Sumathi also provided some of the rate rules used in this work; these will soon be superseded by much-improved versions in separate publications of Dr. Sumathi. We are grateful to Dr. Hans-Heinrich Carstensen, of the Colorado School of Mines, who provided the CHEMDIS input file for the propargyl + propargyl system. The authors also acknowledge helpful interactions with Dr. Preeti Aghalayam, who developed flexible software for initializing the mechanism generation system, and with Prof. Linda J. Broadbelt. This work was financially supported by the Division of Chemical Sciences, Office of Basic Energy Sciences, Office of Energy Research, U.S. Department of Energy, through Grant No. DE-FG02-98ER14914, and an NSF CAREER Award to W.H.G. (No. CTS-9875335).

Supporting Information Available: Rate-constant library, description of our model for the allene−propyne isomerization system, thermodynamic parameters adapted from previous literature for various species, calculation details regarding the ab initio ring-opening beta-scission of 1,3-cyclopentadien-2-yl, and information regarding pressure-dependent network mechanisms in CHEMKIN format (PDF).

References and Notes

(1) Tynnukov, Y. G.; Genkin, M. V.; Genkin, V. N.; Mart′yanov, M. A. *Petr. Chem.* **2002**, *42*, 85.

(2) Li, L.; Borry, R. W.; Iglesia, E. *Chem. Eng. Sci.* **2001**, *56*, 1869−1881.

(3) Tanner, D. D.; Kandanarachchi, P.; Ding, Q.; Shao, H.; Vizitiu, D.; Franz, J. *Energy Fuels* **2001**, *15*, 197−204.

(4) Bobrova, I. I.; Chesnokov, V. V.; Bobrov, N. N.; Zikovskii, V. I.; Parmon, V. N. *Kinet. Catal.* **2000**, *41*, 19−24.

(5) Sun, Q.; Tang, Y.; Gavalas, G. *Energy Fuels* **2000**, *14*, 490−494.

(6) Hidaka, Y.; Sato, K.; Henmi, Y.; Tanaka, H.; Inami, K. *Combust. Flame* **1999**, *118*, 340−358.

(7) Gueret, C.; Daroux, M.; Billaud, F. *Chem. Eng. Sci.* **1997**, *52*, 815−827.

(8) Fedoseev, V. I.; Aristov, Y. I.; Tanashev, Y. Y.; Parmon, V. N. *Kinet. Catal.* **1996**, *37*, 808−811.

(9) Bammidipati, S.; Stewart, G. D.; Elliott J. R.; Gokoglu, S. A.; Purdy, M. J. *AIChE J.* **1996**, *42*, 3123−3132.

(10) Lange, J. P.; Tijm, P. J. A. *Chem. Eng. Sci.* **1996**, *51*, 2379−2387.

(11) Holmen, A.; Olsvik, O.; Rokstad, O. A. *Fuel Process. Technol.* **1995**, *42*, 249−267.

(12) Olsvik, O.; Rokstad, O. A.; Holmen, A. *Chem. Eng. Technol.* **1995**, *18*, 349−358.

(13) Arutyunov, V. S.; Vedeneev, V. I.; Moshkina, R. I.; Ushakov, V. A. *Kinet. Catal.* **1991**, *32*, 234−240.

(14) Faliks, A.; Yetter, R. A.; Floudas, C. A.; Hall, R.; Rabitz, H. *J. Phys. Chem. A* **2000**, *104*, 10740−10746.

(15) Back, M. H.; Back, R. A. In *Pyrolysis: Theory and Industrial Practice*; Albright, L. F., Crynes, B. L., Corcoran, W. H., eds.; Academic Press: New York, 1983; pp 1−24.

(16) Chen, C. J.; Back, M. H.; Back, R. A. *Can. J. Chem.* **1975**, *53*, 3580.

(17) Chen, C. J.; Back, M. H.; Back, R. A. *Can. J. Chem.* **1976**, *54*, 3175−3184.

(18) Roscoe, J. M.; Thompson, M. J. *Int. J. Chem. Kinet.* **1985**, *17*, 967−990.

(19) Dean, A. M. *J. Phys. Chem.* **1990**, *94*, 1432−1439.

(20) Kiefer, J. H.; Tranter, R. S.; Wang, H.; Wagner, A. F. *Int. J. Chem. Kinet.* **2001**, *33*, 834−845.

(21) Roy, K.; Braun-Unkhoff, M.; Frank, P.; Just, Th. *Int. J. Chem. Kinet.* **2001**, *33*, 821−833.

(22) Nguyen, T. L.; Le, T. N.; Mebel, A. M. *J. Phys. Org. Chem.* **2001**, *14*, 131−138.

(23) Wang, H.; Brezinsky, K. *J. Phys. Chem. A* **1998**, *102*, 1530−1541.

(24) Kern, R. D.; Zhang, Q.; Yao, J.; Jursic, B. S.; Tranter, R. S.; Greybill, M. A.; Kiefer, J. H. *Proc. Combust. Inst.* **1998**, *27*, 143−150.

(25) Roy, K.; Horn, C.; Frank, P.; Slutsky, V. G.; Just, T. *Proc. Combust. Inst.* **1998**, *27*, 329−336.

(26) Matheu, D. M.; Aghalayam, P.; Green, W. H., Jr.; Grenda, J. M. Capturing Pressure-Dependence in Automated Mechanism Generation for Pyrolysis and Combustion. Presented at the 17th International Symposium on Gas Kinetics, Essen, Germany, 2002; Paper CO.06.

(27) McMillen, D. F.; Golden, D. M. *Annu. Rev. Phys. Chem.* **1982**, *33*, 493−532.

(28) Tomlin, A. S.; Turányi, T.; Pilling, M. J. In *Low-Temperature Combustion and Autoignition*; Pilling, M. J., ed.; Elsevier: Amsterdam, 1997.

(29) Grenda, J. M.; Androulakis, I. P.; Dean, A. M.; Green, W. H., Jr. *Ind. Eng. Chem. Res.* **2003**, *42*, 1000−1010.

(30) Matheu, D. M. *Integrated Pressure-Dependence in Automated Mechanism Generation: A New Tool for Building Gas-Phase Kinetic Models*, Ph.D. Thesis, Massachusetts Institute of Technology, Cambridge, MA, 2002.
(31) Grenda, J. M.; Bozzelli, J. W. Automated Elementary Reaction Mechanism Generation Incorporating Thermochemistry, Falloff, and Chemical Activation Reactions of OH with Olefins. Presented at the 5th International Conference on Chemical Kinetics, Gaithersburg, MD, 2001; Paper A6.
(32) Broadbelt, L. J.; Stark, S. M.; Klein, M. T. *Ind. Eng. Chem. Res.* **1994**, *33*, 790−799.
(33) Broadbelt, L. J.; Stark, S. M.; Klein, M. T. *Ind. Eng. Chem. Res.* **1995**, *34*, 2566−2573.
(34) Broadbelt, L. J.; Stark, S. M.; Klein, M. T. *Comput. Chem. Eng.* **1996**, *20*, 113−129.
(35) Susnow, R. G.; Dean, A. M.; Green, W. H.; Peczak, P.; Broadbelt, L. J. *J. Phys. Chem. A* **1997**, *101*, 3731−40.
(36) Matheu, D. M.; Green, W. H., Jr.; Grenda, J. M. *Int. J. Chem. Kinet.* **2003**, *35*, 95−119.
(37) Matheu, D. M.; Lada, T. A.; Green, W. H.; Grenda, J. M.; Dean, A. M. *Comput. Phys. Commun.* **2001**, *138*, 237−249.
(38) Petzold L. R. In *Scientific Computing*; Stepleman, R. S., ed.; North−Holland: Amsterdam, 1983; pp 63−68.
(39) Song, J.; Stephanopoulos, G.; Green, W. H. *Chem. Eng. Sci.* **2002**, *57*, 4475−4491.
(40) Chang, A. Y.; Bozzelli, J. W.; Dean, A. M. *Z. Phys. Chem.* **2000**, *214*, 1533−1568.
(41) Bozzelli, J. W.; Chang, A. Y.; Dean, A. M. *Int. J. Chem. Kinet.* **1997**, *29*, 161−170.
(42) Dean, A. M.; Bozzelli, J. W.; Ritter, E. R. *Combust. Sci. Technol.* **1991**, *80*, 63−85.
(43) Dean, A. M. *J. Phys. Chem.* **1985**, *89*, 4600−4608.
(44) Dean, A. M.; Westmoreland, P. R. *Int. J. Chem. Kinet.* **1987**, *19*, 207−228.
(45) Bozzelli, J. W.; Dean, A. M. *J. Phys. Chem.* **1990**, *94*, 3313−3317.
(46) Westmoreland, P. R. *Combust. Sci. Technol.* **1992**, *82*, 151−168.
(47) Yamada, T.; Bozzelli, J. W.; Lay, T. *J. Phys. Chem. A* **1999**, *103*, 7646−7655.
(48) Richter, H.; Mazyar, O. A.; Sumathi, R.; Green, W. H.; Howard, J. B. *J. Phys. Chem. A* **2001**, *105*, 1561−1573.
(49) Sheng, C. Y.; Bozzelli, J. W.; Dean, A. M.; Chang, A. Y. *J. Phys. Chem. A* **2002**, *106*, 7276−7293.
(50) Davis, S. G.; Law, C. K.; Wang, H. *J. Phys. Chem. A* **1999**, *103*, 5889−5899.
(51) Moskaleva, L. V.; Lin, M. C. *J. Comput. Chem.* **2000**, *21*, 415−425.
(52) Matheu, D. M.; Green, W. H., Jr.; Grenda, J. M. *Abstr. Pap.—Am. Chem. Soc.* **2002**, *224*, PHYS-181.
(53) Ritter, E. R.; Bozzelli, J. W. *THERM: Thermo Estimation for Radicals and Molecules*, Version 4.5; New Jersey Institute of Technology, Newark, NJ, 1994.
(54) Ritter, E. R.; Bozzelli, J. W. *Int. J. Chem. Kinet.* **1991**, *23*, 767−778.
(55) Kiefer, J. H.; Mudipalli, P. S.; Sidhu, S. S.; Kern, R. D.; Jursic, B. S.; Xie, K.; Chen, H. *J. Phys. Chem. A* **1997**, *101*, 4057−4071.
(56) Curran, H. J.; Gaffuri, P.; Pitz, W. J.; Westbrook, C. K. *Combust. Flame* **1998**, *114*, 149−177.
(57) Sumathi, R., personal communication, 2002.
(58) Martinez, C.; Cooksy, A. L. *J. Org. Chem.* **2002**, *67*, 2295−2302.
(59) Tsang, W. *J. Phys. Chem. Ref. Data* **1988**, *17*, 887−951.
(60) Tsang, W. *J. Phys. Chem. Ref. Data* **1990**, *19*, 1−68.
(61) Dahm, K. *Hydrocarbon Pyrolysis: Experiments and Graph Theory Modeling*, Ph.D. Thesis, Massachusetts Institute of Technology, Cambridge, MA, 1998.
(62) Knyazev, V.; Slagle, I. R. *J. Phys. Chem. A* **2002**, *106*, 5613−5617.
(63) Tsang, W. *J. Phys. Chem. Ref. Data* **1991**, *20*, 221−273.
(64) Allara, D. L.; Shaw, R. *J. Phys. Chem. Ref. Data* **1980**, *9*, 523−559.
(65) Kee, R. J.; Rupley, F. M.; Miller, J. A.; Coltrin, M. E.; Grcar, J. F.; Meeks, E.; Moffat, H. K.; Lutz, A. E.; Dixon-Lewis, G.; Smooke, M. D.; Warnatz, J.; Evans, G. H.; Larson, R. S.; Mitchell, R. E.; Petzold, L. R.; Reynolds, W. C.; Caracotsios, M.; Stewart, W. E.; Glarborg, P.; Wang, C.; Adigun, O. CHEMKIN Collection, Version 3.6; San Diego, CA, 2000.
(66) Bossard, A. R.; Back, M. H. *Can. J. Chem.* **1991**, *68*, 1401−1407.
(67) Bossard, A. R.; Back, M. H. *Can. J. Chem.* **1990**, *69*, 37−42.
(68) Chen, C. J.; Back, M. H.; Back, R. A. *Can. J. Chem.* **1977**, *55*, 1624−1628.
(69) Miller, J. A.; Melius, C. F. *Combust. Flame* **1992**, *91*, 21−39.
(70) Carstensen, H.-H. CHEMDIS Input File for Propargyl + Propargyl System, unpublished work, 2002.
(71) Knyazev, V. D.; Slagle, I. R. *J. Phys. Chem. A* **2001**, *105*, 3196−3204.
(72) James, D. G. L.; Troughton, G. E. *Trans. Faraday Soc.* **1966**, *62*, 145.